

ORIGINAL ARTICLE

Impact of Attenuation Correction, Collimator, and Iterative Reconstruction Protocols on ^{67}Ga SPECT/CT Quantification

Sahar Rezaei ^{1,2}, Saeed Farzanehfar ³, Leyla Badrzadeh ³, Faezeh Assadi ³, Nasim Vahidfar ³, Peyman Sheikhzadeh ^{3*} 

¹ Department of Nuclear Medicine, Medical School, Tabriz University of Medical Sciences, Tabriz, Iran

² Clinical Research Development Unit, Imam Reza General Hospital, Tabriz University of Medical Sciences, Tabriz, Iran

³ Department of Nuclear Medicine, Imam Khomeini Hospital Complex, Tehran University of Medical Sciences, Tehran, Iran

*Corresponding Author: Peyman Sheikhzadeh

Received: 13 October 2022 / Accepted: 25 December 2022

Email: sheikhzadeh-p@sina.tums.ac.ir

Abstract

Purpose: The main goal of this study was to determine the optimal collimator in the absence of medium energy collimators along with the impact of Attenuation Correction (AC) and different iterative reconstruction protocols on the quantitative evaluation of Gallium-67 SPECT/CT imaging.

Materials and Methods: A GE Discovery 670 dual-head SPECT/CT scanner and a NEMA phantom filled with ^{67}Ga solution were used to scan the patients. The projections were acquired with both Low Energy High Resolution (LEHR) and High Energy General Purpose (HEGP) collimators, and CT images were acquired to evaluate the effect of attenuation correction. SPECT data were reconstructed using the Ordered Subset Expectation Maximization (OSEM) method with various combinations of iterations and subsets. The performance was quantified, and a clinical study validated the phantom study.

Results: Acquired images by the HEGP collimator yielded higher Contrast Recovery (CR) and Contrast to Noise Ratio (CNR) in images with AC than those without non-AC (41.6% and 74.2%, respectively). The CNR in all spheres after AC was increased by 80.4% (82.1%) for the HEGP collimator against the LEHR collimator. Also, an increase in iterations \times subsets from 16 to 48 led to the Coefficient of Variation (COV) increasing by 17.2%, 16.67%, 15.50%, 14.4%, 14.2%, and 14.1% for 10 mm to 37 mm sphere diameter, respectively.

Conclusion: CT-based AC and HEGP collimators can yield improved ^{67}Ga SPECT quantification compared to Non-AC and LEHR collimators. The choice of the optimal collimator with the reconstruction protocol led to changes in the image quality and quantitative accuracy, emphasizing the need to carefully select the appropriate combination of data acquisition factors.

Keywords: ^{67}Ga -Citrate; Attenuation Correction; Iterative Reconstruction; Quantitative Imaging; Single Photon Emission Computed Tomography; Computed Tomography.

1. Introduction

Single-Photon Emission Computed Tomography (SPECT) imaging is one of the most important tools for many clinical tasks, including lesion detection, staging, and therapy response monitoring [1, 2]. However, this modality's image quality and quantitative accuracy are affected by the acquisition and reconstruction protocols, which are closely associated with the collimator, photopeak definition, and corrections [3-5]. In this regard, photon attenuation in a patient's body is a degradation factor limiting diagnostic or prognostic accuracy. This can diminish the accuracy and specificity of perfusion defect detection using SPECT imaging [6, 7]. Hybrid SPECT/CT scanners allow the direct fusion of high-resolution anatomical structures and functional images and produce attenuation correction maps.

Moreover, in recent years, iterative reconstruction algorithms with a progressive variety of reconstruction schemes that are upgraded by incorporating attenuation correction, physical modeling of the collimator and detector, and point spread function modeling are very popular in nuclear medicine [8, 9]. In myocardial perfusion imaging, clinical studies [10-12] have reported that iterative reconstruction algorithms can influence quantitative evaluation. They also indicated that image quality and sensitivity improved after using iterative reconstruction algorithms with attenuation correction. Furthermore, the reconstruction and acquisition parameters can affect SPECT-based quantification. Previous studies [13, 14] have shown that an appropriate reconstruction protocol selection can lead to better lesion characterization and an improved clinical interpretation, particularly in small and low-uptake lesions.

^{67}Ga is a cyclotron-produced radionuclide with remarkable physical characteristics for diagnostic applications in nuclear medicine [15]. Its gamma radiation, including (93 keV (39%), 184 keV (21%), 296 keV (22%), and 378 keV (7%)) in an appropriate range of imaging studies (30-300 keV) with adequate abundances make SPECT diagnostic studies possible [16]. ^{67}Ga has been used to detect various solid tumors since 1969 [15]. [^{67}Ga]Ga-citrate is commonly used to assess chronic infections (such as sarcoidosis), evaluate interstitial lung disease, and examine patients with Acquired Immunodeficiency Syndrome (AIDS) [15, 17, 18]. Another substantial role of [^{67}Ga] Ga-citrate as an imaging tracer is diagnosing neoplastic disease, mostly for

evaluating lymphoma [15, 19, 20]. The longer half-life of ^{67}Ga compared to technetium-99m ($^{99\text{m}}\text{Tc}$) (78.25 h and 6 h, respectively) can be a brilliant point that helps establish long-period imaging studies [21]. Recently, a preclinical study of a newly designed radiopharmaceutical of ^{67}Ga was published ([^{67}Ga]Ga-phytate) [21], which demonstrated the importance of the longer half-life of ^{67}Ga in lymphoscintigraphy of breast malignancies. The results were the same as those achieved with $^{99\text{m}}\text{Tc}$ -labeled colloids with the possibility of longer period imaging studies [21]. It would be promising if this tracer could be developed in clinical trials as an alternative to $^{99\text{m}}\text{Tc}$ radiopharmaceuticals [22].

Due to ^{67}Ga multiple-energy emissions, lesion detectability is widely affected by large scatter events within the photopeak energy window [23, 24]. In this regard, Farncombe *et al.* reported that lesion contrast degrades due to the additional down scatter of high-energy photons into lower-energy acquisition windows [25]. On the other hand, the image quality and quantitative accuracy of ^{67}Ga studies decline, particularly due to incorrect collimator choice. Previous studies had demonstrated that spatial resolution and contrast in ^{67}Ga imaging deteriorated when a low-energy collimator was applied because of the presence of higher septal penetration and scattered photons [26]. In a recent study, Ouahman *et al.* [27] evaluated the influence of the collimator and energy window on the ^{67}Ga point source using a Monte Carlo simulation. A Low-Energy High-Resolution (LEHR) collimator resulted in a lower spatial resolution. Furthermore, they stated that a High-Energy General Purpose (HEGP) collimator could cause lower sensitivities and lower spatial resolutions.

In clinical situations, visual assessment of normal tissue-to-tumor ratios has an important role to play, apart from quantitative analysis. More importantly, the image contrast, noise, and spatial resolution are hampered in small and low-uptake lesions. To improve image quality and quantitative accuracy and reduce decision-making mistakes in SPECT studies, factors that contribute to the abovementioned factors should be recognized and optimized. To our knowledge, no study has simultaneously evaluated the impact of AC, collimator, and iterative reconstruction protocols on ^{67}Ga SPECT/CT quantification. Therefore, the first aim of this study was to survey the effects of attenuation correction and determine the optimum collimator. The second aim of this study was to assess the effects of various iterative reconstruction

parameters on ⁶⁷Ga SPECT quantification after choosing the optimal collimator.

2. Materials and Methods

2.1. Phantom Image Acquisition and Reconstruction

The phantom study was performed using a NEMA IEC body image quality phantom. Six spheres of the NEMA phantom (inner diameters: 10, 13, 17, 22, 28, and 37 mm; wall thickness: ~ 1 mm) were filled with ⁶⁷Ga solution with a Sphere-to-Background Ratio (SBR) of 10:1. A cylindrical lung insert was placed at the center of the phantom. A background activity level of 5.3 kBq/mL was used in the phantom study.

Data were acquired using Discovery 670 SPECT/CT (GE Healthcare, Milwaukee, Wisconsin, USA) with two collimator types: LEHR and HEGP. Scans were acquired over 360° at 40 views (20 s/view, step and shoot mode, 180° detector configuration) in a 64 × 64 matrix with a pixel size of 6.64 mm and a noncircular orbit. Three main energy windows were defined: one at 93 keV with a 13% width, one at 185 keV, and one at 300 keV with a 10% width. All SPECT data were reconstructed using the Ordered Subset Expectation Maximization (OSEM) algorithm with Attenuation Correction (AC) and without attenuation correction (non-AC) with 2 and 3 iterations, and 8, 12, and 16 subsets with 2, 4, and 6 mm Gaussian post-smoothing filters. CT imaging was performed for attenuation correction using 120 kVp, 40 mA, and 512 × 512 matrix size with 5 mm slice thickness. Furthermore, the "Cardiac AC Low Dose Chest Spiral Acquisition" CT protocol was applied.

2.2. Patient Study

The phantom study was validated through clinical studies. In this study, ⁶⁷Ga SPECT/CT images of two patients (two 61- and 50-year-old females) were retrospectively evaluated. For validation, the default image reconstruction setting was the same as our previous phantom study. For comparison, the datasets were reconstructed using various iterative reconstruction protocols.

2.3. Imaging Analysis

Image quality was assessed using Contrast Recovery (CR), Coefficient of Variation (COV), and Contrast to Noise Ratio (CNR). The CR was calculated as follows (Equation 1):

$$CR = \frac{\frac{C_j}{C_{bkg}} - 1}{SB_{ratio} - 1} \times 100\% \quad (1)$$

Where C_j and C_{bkg} are the mean values of the sphere, and background Volumes Of Interest (VOIs), respectively, and SB_{ratio} represents the actual SBR. The COV was given by (Equation 2):

$$COV = \frac{\sigma_{bkg}}{C_{bkg}} \times 100\% \quad (2)$$

Where σ_{bkg} is the mean, Standard Deviation (SD) of the intensity values in the background VOI. Additionally, the CNR was calculated as the ratio of the mean value of a VOI of the sphere minus the mean value in the background VOIs over the mean SD in the background VOIs, that is (Equation 3),

$$CNR = \frac{C_j - C_{bkg}}{\sigma_{bkg}} \quad (3)$$

The VOIs were determined based on the CT images. The relative difference (%) was also applied to compare the quantitative values of the various collimators. It's important to note that all corrections (scatter, attenuation, and resolution) were considered in performing the image evaluation.

3. Results

A comparison between the NEMA phantom images obtained by both collimators with and without attenuation correction is depicted in Figure 1. The application of attenuation correction led to a decline in the COV values compared to the case without attenuation correction in both the LEHR and HEGP collimators.

The CR and CNR for the images with and without AC in all spheres for the LEHR and HEGP collimators are shown in Figure 2. Higher CR yielded images with AC with a greater impact on the HEGP collimator relative to the LEHR collimator. Furthermore, a CR

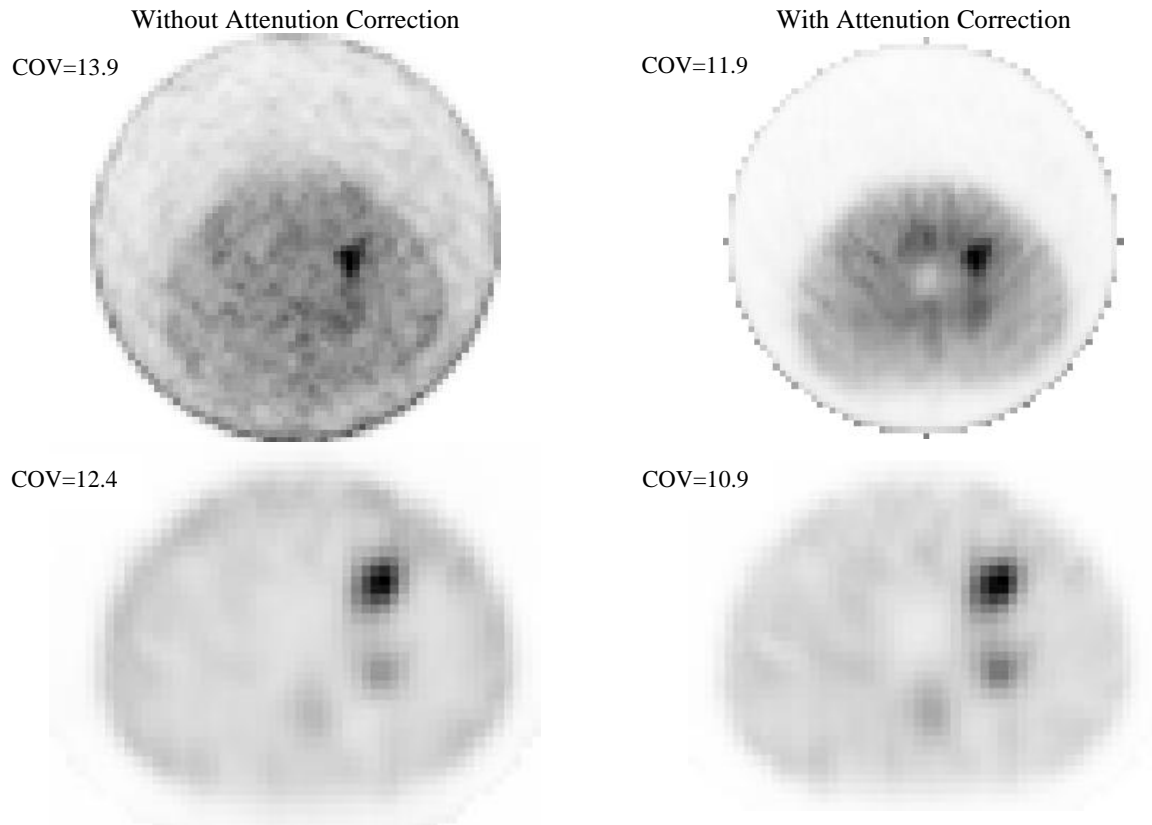


Figure 1. Phantom data. Images of NEMA phantom with; First row: LEHR, second row: HEGP collimators
COV: Coefficient of variation, LEHR: Low-energy high-resolution, HEGP: High energy general purpose

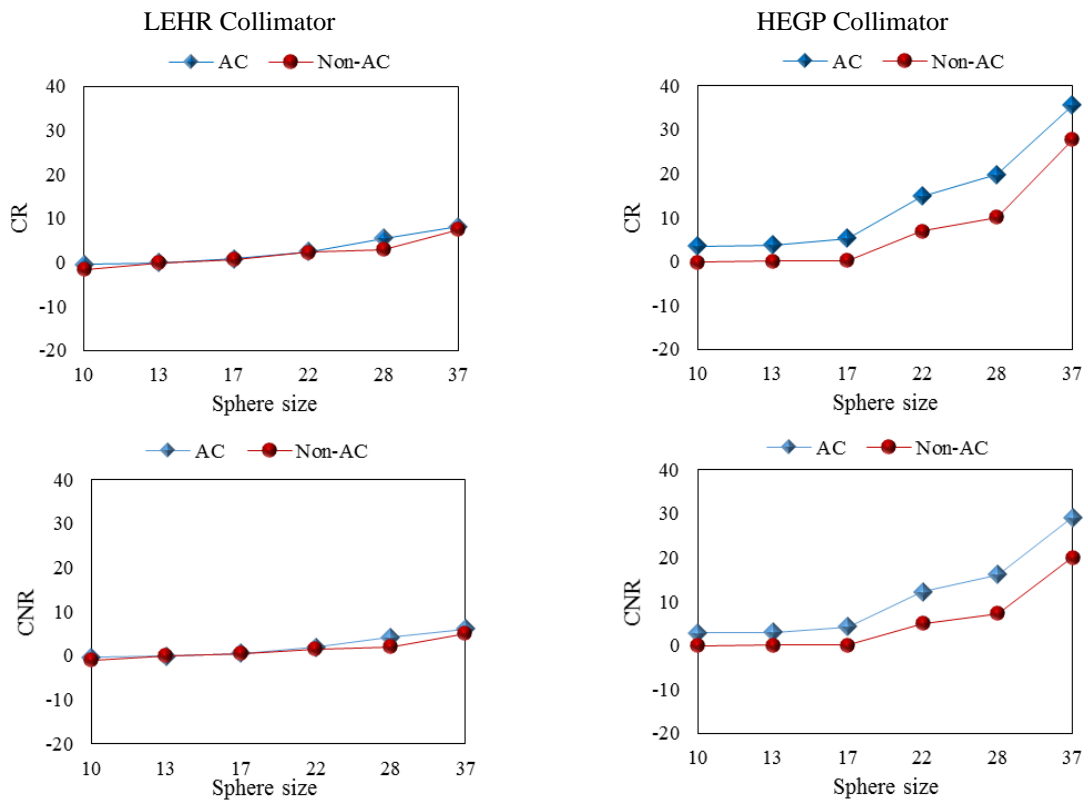


Figure 2. Phantom data. Comparison between CR (first row) and CNR (second row) of the NEMA phantom spheres before and after attenuation correction (AC). All data were reconstructed with two iterations and twelve subsets with a 2 mm Gaussian filter

improvement was observed for the larger hot spheres with higher intensity. The mean relative CR for larger spheres (sizes: 22, 28, and 37 mm diameter) in images with AC compared to the corresponding images without AC was increased by 19.9% and 41.6% for LEHR and HEGP collimators, respectively. Overall, the CNR with attenuation correction was higher than that of without attenuation correction. The mean relative differences (%) of the CNR values of all spheres in images with AC compared to the corresponding images without AC were 53.5% and 74.2% for LEHR and HEGP collimators, respectively.

It can also be seen that for both AC and non-AC conditions, the HEGP collimator yielded a higher CNR compared to the LEHR collimator. To evaluate the impact of various collimators on SPECT images, the CR and CNR were compared after attenuation correction (Figure 3). For all spheres after AC, the HEGP collimator yielded a higher CR and CNR than the LEHR collimator. Furthermore, the mean CR (CNR) in all spheres was increased by 80.4% (82.1%) for the HEGP collimator compared to the LEHR collimator. Thus, the mean CR and CNR significantly improved for all spheres after the HEGP collimator was used.

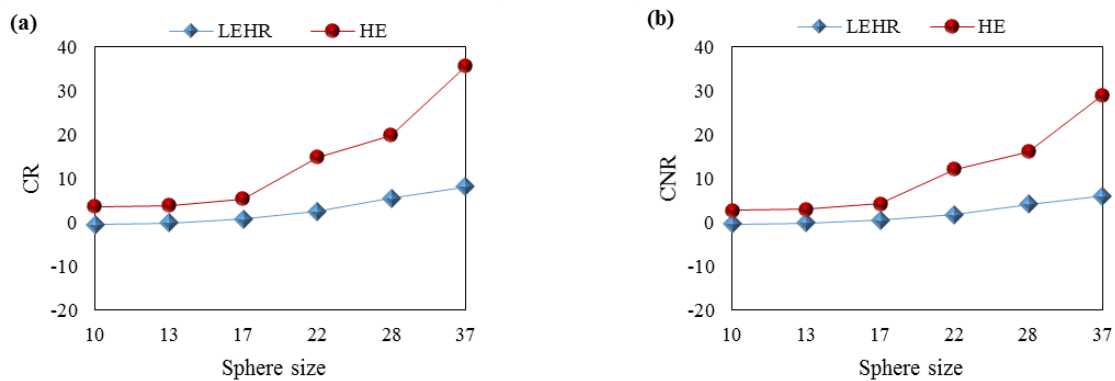


Figure 3. Phantom data. Comparison between LEHR and HEGP collimators in various NEMA phantom spheres after attenuation correction (AC) (a): CR, (b): CNR. All data were reconstructed with two iterations and twelve subsets with a 2 mm Gaussian filter

Figure 4 compares the various reconstruction parameters in terms of CR, CNR, and COV. In all spheres, higher iterations and subsets provided a higher CR and lowered CNR than the lower ones. The relative difference (%) between the minimum and maximum of CR (CNR) with the increase in iterations \times subsets from 16 to 48 were 31.4% (-19.2%) for 10 mm sphere diameter, 30.0% (-22.7%) for 13 mm sphere diameter, 31.5% (-22.4%) for 17 mm sphere

diameter, 31.6% (-25.0%) for 22 mm sphere diameter, 27.5% (-26.3%) for 28 mm sphere diameter, and 24.9% (-27.9%) for 37 mm sphere diameter. Furthermore, in all iterations and subsets, a higher variation was seen for smaller spheres than for the larger spheres. An increase in iterations \times subsets from 16 to 48 led to the COV increasing by 17.2%, 16.67%, 15.50%, 14.4%, 14.2%, and 14.1% for 10 mm, 13 mm, 17 mm, 22 mm, 28 mm, and 37 mm sphere diameters, respectively.

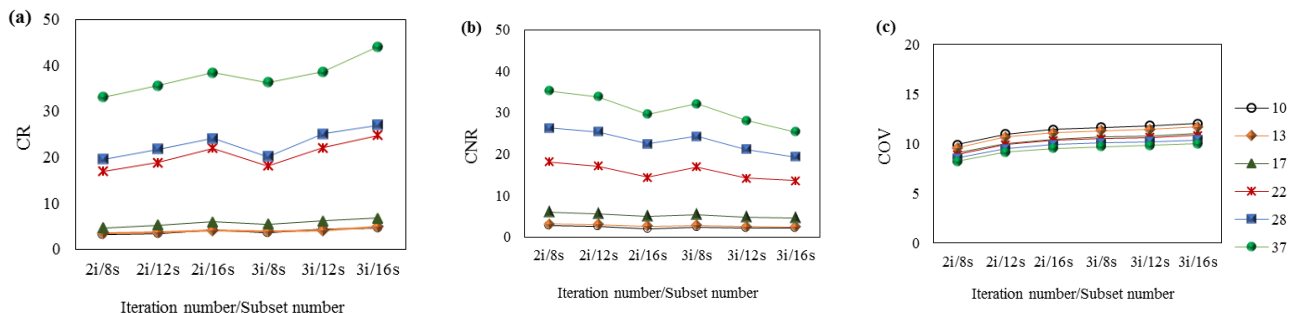


Figure 4. Phantom data. Comparison between various reconstruction protocols in different NEMA phantom spheres; (a): CR, (b): CNR, (c): COV. A 2 mm Gaussian filter was used for all reconstructions
CR: Contrast recovery, CNR: Contrast-to-noise-ratio, COV: Coefficient of variation

A comparison between the NEMA phantom images for various Gaussian filters is depicted separately for different iterations and subsets, as shown in Figure 5. Although applying the post-smoothing filter led to the decline of the COV, in various reconstruction protocols, the blurring effect was increased by increasing the post-smoothing filter size.

Using various protocols, two ^{67}Ga SPECT/CT clinical datasets were reconstructed for the quantitative assessment. Figure 6 shows images of patients with infection effects. As anticipated, CR increased with increasing iterations and subsets. Consequently, the clinical findings follow the phantom results.

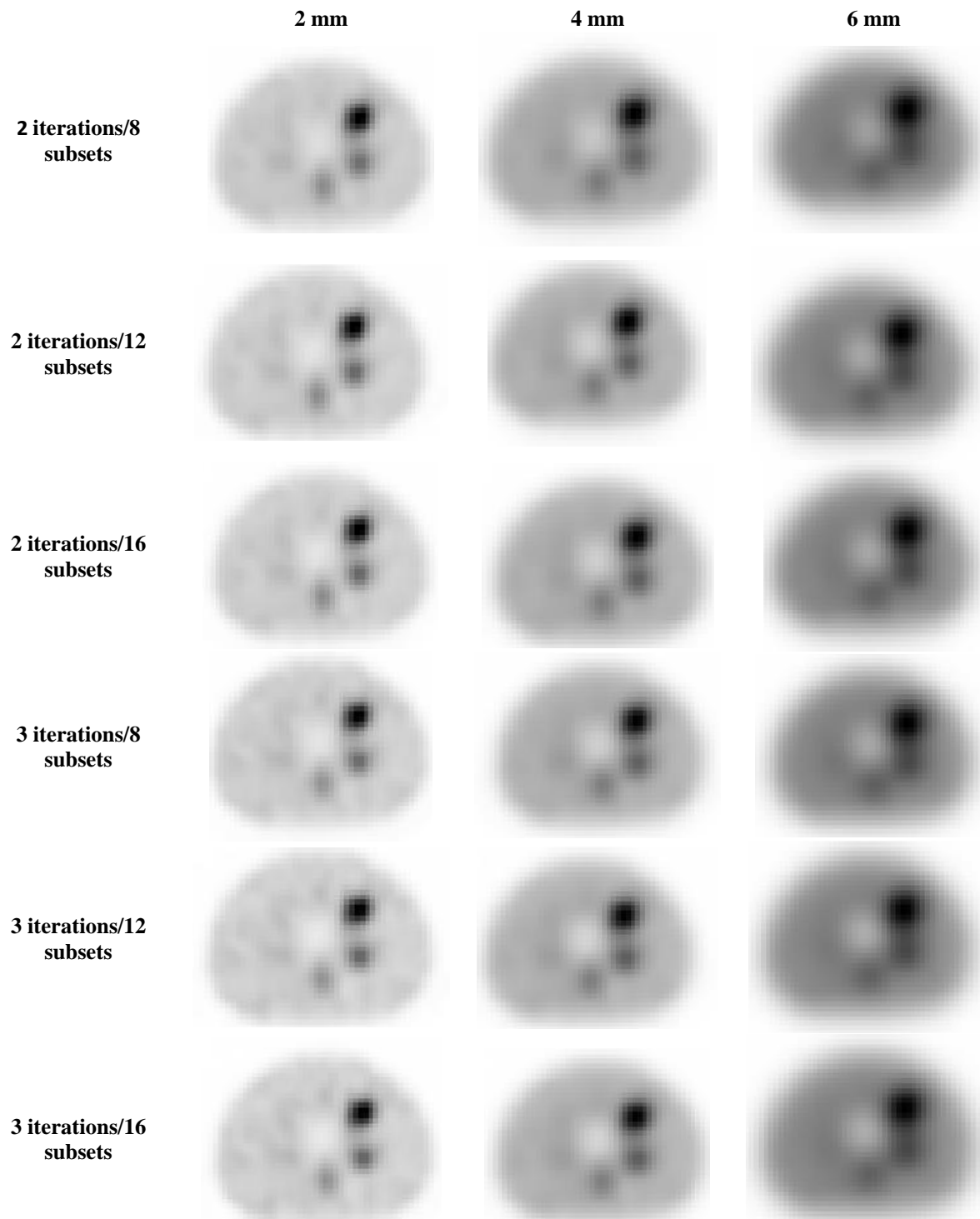


Figure 5. Reconstructed NEMA phantom images with various reconstruction parameters and filter sizes. HEGP collimator was used for data acquisition

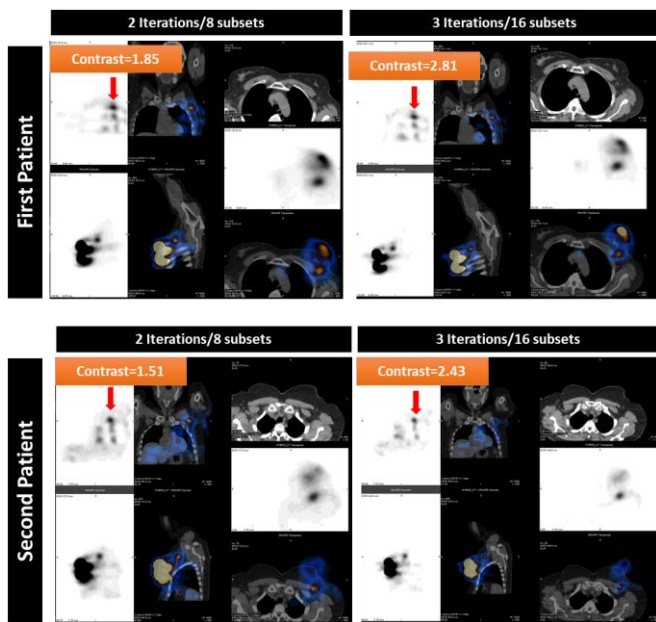


Figure 6. Patient data. ^{67}Ga SPECT images of patients with infection; First row: Coronal images of a 61-years-old female. Second row: Coronal images of a 50-years-old female. HEGP collimator was used for data acquisition

4. Discussion

In ^{67}Ga SPECT/CT studies, deterioration in image quality due to multiple-energy rays of ^{67}Ga , and consequently large scatter events within the photopeak energy window, presents a potential challenge. Given the variety of collimators, the choice of an inappropriate collimator can degrade quality and quantity factors. Furthermore, the importance of iterative reconstruction protocols and attenuation correction is unclear for ^{67}Ga studies. We assessed the impact of various reconstruction protocols and attenuation correction to address these challenges by quantitatively evaluating NEMA phantom images with both LEHR and HEGP collimators. The issue that should be noted is that many centers, such as ours, do not have a medium-energy collimator; therefore, choosing the type of collimator among HEGP and LEHR and optimizing the reconstruction protocol is important.

Our phantom study demonstrated that applying the HEGP collimator can improve image quality with a greater impact on images with attenuation correction than without attenuation correction (Figure 1). Another observation is that incorporating AC into the iterative reconstruction algorithm can decrease the noise levels. Although attenuation correction can improve image quality, CT-based AC maps are highly sensitive to involuntary or voluntary patient movements, which may

cause misalignment errors between emission and transmission scans and, ultimately, quantitative uncertainty or image artifacts.

Our phantom study demonstrated that the highest CR was 35.5 for the HEGP collimator with AC reconstruction in a 37 mm sphere (Figure 2). Generally, in both images with AC and non-AC, the CR of the 37 mm sphere was the highest, and applying the LEHR collimator decreased the CR. For the HEGP collimator, the mean CR for all the spheres was 13.7 for AC and 7.43 for non-AC. The mean CR values of the LEHR collimator for images with and without AC were 2.6 and 1.9, respectively.

We also observed that higher CNR values for both collimators in ^{67}Ga imaging were obtained for all spheres in the AC images (Figure 2). Previous studies have shown that incorporating AC in reconstruction algorithms can lead to improved contrast-noise trade-off performance relative to non-AC algorithms [28, 29]. Similar to the HEGP collimator, the larger spheres in the images obtained with the LEHR collimator resulted in a higher CNR. In this regard, Huizing *et al.* mentioned that lower counts and, consequently, noise amplification for radionuclides with multiple-energy emissions could decrease the quantitative accuracy depending on the collimator and energy window, particularly in small and low-uptake lesions [4].

It can be seen that the CR and CNR values decreased by applying LEHR collimators for all spheres in the AC images (Figure 3), which was due to the large scatter events within the ^{67}Ga photopeak energy window. Furthermore, with a decrease in sphere size from 37 to 10 mm in diameter, both the CR and CNR decreased. In general, quantitative SPECT imaging and Ga SPECT imaging, particularly, suffer from limited spatial resolution, which is closely related to collimator blurring. Previous studies have shown that the impact of PVE and spatial resolution can lead to diminished quantification accuracy and reliability, particularly for small lesions.

Our results indicate that more iterations and subsets can lead to improved CR (Figure 4). This is consistent with other studies showing that image quality and quantification precision improved when higher iterations and subsets were used [24, 25]. However, the CNR values decreased with an increase in the number of iterations and subsets due to noise level enhancements (Figure 4). The dependency of CNR on reconstruction

parameters is in agreement with previous studies showing that CNR measurements can be affected by reconstruction parameters [26, 27]. Furthermore, increased iterations and subsets observed notable variations in CR and CNR among different protocols. In the phantom study performed by Rezaei *et al.* [13], noteworthy degradations of CNR values were also reported when using higher iterations and subsets. Apart from the phantom studies that have been applied and contributed to choosing a suitable collimator and reconstruction factors for ^{67}Ga SPECT quantification, our validation study with two clinical studies also demonstrated that performing HEGP collimator as well as higher iterations \times subsets led to the production of better images (Figure 6).

Due to the multiple-energy rays emitted by ^{67}Ga , a large scattering event is observed within the photopeak energy window; this event compromises lesion detection and contrast significantly [30]. When there is a high level of penetrated and scattered photons from the LEHR collimator, spatial resolution, contrast, and quantification are impaired [31]. Therefore, may me ^{67}Ga imaging with a single peak could provide higher quality, but the best way for optimizing the number and width of the energy window in different collimators is the Monte Carlo simulation, which is our future work.

The present work highlights the impact of collimator and reconstruction protocol selection, along with reconstruction protocols, on quantitative accuracy in ^{67}Ga SPECT images with and without attenuation correction. In summary, we found that quantification accuracy and reliability were affected by data acquisition, reconstruction protocols, and lesion size, and with decreasing lesion size, these effects were highlighted. These findings suggest that collimators and reconstruction protocols should be chosen carefully when applying radionuclides with multiple energy emissions.

A limitation of our study is that all measurements for the NEMA phantom were performed only with a 10:1 sphere-to-background ratio and fixed background activity. Another limitation is that with phantom data, we did not evaluate the medium-energy collimator or the impact of this parameter on the metric values.

5. Conclusion

The study demonstrates that using the HEGP collimator, and in particular, incorporation of attenuation correction, can improve both the visual interpretation and quantitative analysis of ^{67}Ga SPECT/CT compared to Non-AC and LEHR collimators. Our results prove that ^{67}Ga SPECT/CT quantitation accuracy depends on collimator selection, lesion size, and reconstruction protocols. Choosing the appropriate combination of data acquisition and reconstruction protocols must be carefully specified.

Acknowledgements

We would like to thank all technologists of the PET-CT department in Imam Khomeini Hospital Complex (IKHC) in Tehran, Iran for helping to provide the data.

References

- 1- Ora Israel *et al.*, "Two decades of SPECT/CT—the coming of age of a technology: an updated review of literature evidence." *European journal of nuclear medicine and molecular imaging*, Vol. 46 (No. 10), pp. 1990-2012, (2019).
- 2- Michael Vaiman *et al.*, "Low-radiation of technetium-99m-sestamibi and single-photon emission computed tomography/computed tomography to diagnose parathyroid lesions." *World journal of nuclear medicine*, Vol. 18 (No. 1), p. 52, (2019).
- 3- Taher Hosny, Magdy M Khalil, Abdo A Elfiky, and Wael M Elshemey, "Image quality characteristics of myocardial perfusion SPECT imaging using state-of-the-art commercial software algorithms: evaluation of 10 reconstruction methods." *American Journal of Nuclear Medicine and Molecular Imaging*, Vol. 10 (No. 6), p. 375, (2020).
- 4- Daphne MV Huizing, Michiel Sinaasappel, Marien C Dekker, Marcel PM Stokkel, and Berinda J de Wit-van der Veen, " ^{177}Lu SPECT/CT: Evaluation of collimator, photopeak and scatter correction." *Journal of Applied Clinical Medical Physics*, Vol. 21 (No. 9), pp. 272-77, (2020).
- 5- Rene Nkoulou *et al.*, "High efficiency gamma camera enables ultra-low fixed dose stress/rest myocardial perfusion imaging." *European Heart Journal-Cardiovascular Imaging*, Vol. 20 (No. 2), pp. 218-24, (2019).
- 6- NV Denisova and MM Ondar, "Effect of attenuation correction on image quality in emission tomography." in *AIP Conference Proceedings*, (2017), Vol. 1893 (No. 1): AIP Publishing LLC, p. 030015.
- 7- Seyed Ali Mirshahvalad, Mohammadreza Chavoshi, and Sepideh Hekmat, "Diagnostic performance of prone-only

- myocardial perfusion imaging versus coronary angiography in the detection of coronary artery disease: A systematic review and meta-analysis." *Journal of Nuclear Cardiology*, pp. 1-13, (2020).
- 8- Michael Ljungberg and P Hendrik Pretorius, "SPECT/CT: an update on technological developments and clinical applications." *The British journal of radiology*, Vol. 91 (No. 1081), p. 20160402, (2018).
- 9- Meysam Tavakoli and Marian Najj, "Quantitative evaluation of the effect of attenuation correction in SPECT images with CT-derived attenuation." in *Medical Imaging 2019: Physics of Medical Imaging*, (2019), Vol. 10948: *International Society for Optics and Photonics*, p. 109485U.
- 10- Brian G Abbott *et al.*, "Contemporary cardiac SPECT imaging—innovations and best practices: an information statement from the American Society of Nuclear Cardiology." *Circulation: Cardiovascular Imaging*, Vol. 25 (No. 5), pp. 1847-60, (2018).
- 11- Shimpei Ito *et al.*, "Comparison of CTAC and prone imaging for the detection of coronary artery disease using CZT SPECT." *Annals of nuclear medicine*, Vol. 31 (No. 8), pp. 629-35, (2017).
- 12- Tim Van den Wyngaert, Filipe Elvas, Stijn De Schepper, John A Kennedy, and Ora Israel, "SPECT/CT: Standing on the shoulders of giants, it is time to reach for the sky!" *Journal of Nuclear Medicine*, Vol. 61 (No. 9), pp. 1284-91, (2020).
- 13- Sahar Rezaei, Pardis Ghafarian, Abhinav K Jha, Arman Rahmim, Saeed Sarkar, and Mohammad Reza Ay, "Joint compensation of motion and partial volume effects by iterative deconvolution incorporating wavelet-based denoising in oncologic PET/CT imaging." *Physica Medica*, Vol. 68pp. 52-60, (2019).
- 14- Sahar Rezaei *et al.*, "The impact of iterative reconstruction protocol, signal-to-background ratio and background activity on measurement of PET spatial resolution." *Japanese journal of radiology*, Vol. 38 (No. 3), pp. 231-39, (2020).
- 15- Emilio BOMBARDIERL, Cumali AKTOLUN, Richard P BAUM, Angelika BISHOL-DELALOYE, John BUSCOMBE, and Jean Francois CHATAL, "⁶⁷Ga scintigraphy: procedure guidelines for tumour imaging." *European journal of nuclear medicine and molecular imaging Print*, Vol. 30 (No. 12), pp. BP125-BP31, (2003).
- 16- Håkan Hall *et al.*, "In vitro autoradiography of carcinoembryonic antigen in tissue from patients with colorectal cancer using multifunctional antibody TF2 and ^{67/68}Ga-labeled haptens by pretargeting." *American journal of nuclear medicine and molecular imaging*, Vol. 2 (No. 2), p. 141, (2012).
- 17- TATSUYA Miyamae, MASAYASU Kan, MUTSUMI Fujioka, KOUICHI Okada, YASUYUKI Yoshikawa, and JUNICHI Nishikawa, "⁶⁷Ga-citrate scanning in hypernephroma." *Clinical nuclear medicine*, Vol. 3 (No. 6), pp. 225-28, (1978).
- 18- O Bělohávek, J Brousil, J Pradáčová, V Votava, and Z Voslářová, "Objective assessment of ⁶⁷Ga-citrate accumulation in lungs as an expression of sarcoidosis activity." (1989).
- 19- F Zayas *et al.*, "⁶⁷Ga-citrate distribution in solid hepatoma 22." *European journal of nuclear medicine*, Vol. 9 (No. 4), pp. 157-60, (1984).
- 20- Tomomitsu Higashi, Katuo Ito, Kaizo Shimura, Yukihiko Kinoshita, and Sakae Sakurai, "Clinical evaluation of ⁶⁷Ga-citrate scanning in the oral region." *Oral Surgery, Oral Medicine, Oral Pathology*, Vol. 40 (No. 5), pp. 691-99, (1975).
- 21- Zeinab Bayat *et al.*, "Preparation and validation of [⁶⁷Ga] Ga-phytate kit and Monte Carlo dosimetry: An effort toward developing an impressive lymphoscintigraphy tracer." *Journal of Radioanalytical and Nuclear Chemistry*, Vol. 331 (No. 2), pp. 691-700, (2022).
- 22- Meral T Ercan, Tülin Aras, Erkan Ünlenen, Mustafa Ünlü, Işıl S Ünsal, and Zafer Haşçelik, "^{99m}Tc-citrate versus ⁶⁷Ga-citrate for the scintigraphic visualization of inflammatory lesions." *Nuclear medicine and biology*, Vol. 20 (No. 7), pp. 881-87, (1993).
- 23- Irène Buvat, "Methodologies for quantitative SPECT." in *Physics of PET and SPECT Imaging: CRC Press*, (2017), pp. 217-32.
- 24- TH Farncombe, HC Gifford, MV Narayanan, PH Pretorius, EC Frey, and MA King, "Assessment of Scatter Compensation Strategies for ⁶⁷Ga SPECT Using Numerical Observers and Human LROC Studies." *Journal of Nuclear Medicine*, Vol. 45 (No. 5), pp. 802-12, (2004).
- 25- TH Farncombe *et al.*, "An optimization of reconstruction parameters and investigation into the impact of photon scatter in /sup ⁶⁷/Ga SPECT." *IEEE Transactions on Nuclear Science*, Vol. 49 (No. 5), pp. 2148-54, (2002).
- 26- SC Moore, MF Kijewski, and MF Fakhri, "Collimator optimization for detection and quantitation tasks: application to gallium-67 imaging." *IEEE Transactions on Medical Imaging*, Vol. 24 (No. 10), pp. 1347-56, (2005).
- 27- Mina Ouahman *et al.*, "Collimator and Energy Window Evaluation in Ga-67 Imaging by Monte Carlo Simulation." *Molecular imaging and radionuclide therapy*, Vol. 29 (No. 3), p. 118, (2020).
- 28- Laura Demino, Paulo Ferreira, Francisco PM Oliveira, and Durval C Costa, "Comparison of the ⁹⁰Y-labelled glass microspheres liver radioembolisation dosimetry with the estimated dosimetry obtained from pre-treatment ^{99m}Tc-MAA SPECT images reconstructed with and without attenuation correction." *Computer Methods in Biomechanics and Biomedical Engineering: Imaging & Visualization*, Vol. 7 (No. 5-6), pp. 651-59, (2018).
- 29- Tobias Rydén, Martijn Van Essen, Ida Marin, Johanna Svensson, and Peter Bernhardt, "Deep-Learning Generation of Synthetic Intermediate Projections Improves ¹⁷⁷Lu SPECT Images Reconstructed with Sparsely Acquired

Projections." *Journal of Nuclear Medicine*, Vol. 62 (No. 4), pp. 528-35, (2021).

30- Youssef Bouzekraoui, Farida Bentayeb, Hicham Asmi, and Faustino Bonutti, "Energy window and contrast optimization for single-photon emission computed tomography bremsstrahlung imaging with yttrium-90." *Indian journal of nuclear medicine: IJNM: the official journal of the Society of Nuclear Medicine, India*, Vol. 34 (No. 2), p. 125, (2019).

31- Hicham Asmi, Farida Bentayeb, Youssef Bouzekraoui, Faustino Bonutti, and Sanae Douama, "Energy window and collimator optimization in lutetium-177 single-photon emission computed tomography imaging using Monte Carlo simulation." *Indian journal of nuclear medicine: IJNM: the official journal of the Society of Nuclear Medicine, India*, Vol. 35 (No. 1), p. 36, (2020).